Interfacing Strong Electron Acceptors with Single Wall Carbon Nanotubes

Christian Oelsner,[†] Cordula Schmidt,[‡] Frank Hauke,[‡] Maurizio Prato,[#] Andreas Hirsch,*[,‡] and Dirk M. Guldi*[,†]

[†]Department of Chemistry and Pharmacy & Interdisciplinary Center for Molecular Materials (ICMM), Friedrich-Alexander-Universität Erlangen-Nürnberg, Egerlandstrasse 3, 91058 Erlangen, Germany

[‡]Department of Chemistry and Pharmacy, Friedrich-Alexander-Universität Erlangen-Nürnberg, Henkestrasse 42, 91054 Erlangen, Germany

[#]Center of Excellence for Nanostructured Materials, Università degli Studi di Trieste, Dipartimento di Scienze Farmaceutiche Piazzale Europa 1, 34127 Trieste, Italy

Ⓢ *Supporting Information*

ABSTRACT: The complementary use of steady-state and time-resolved spectroscopy in combination with electrochemistry and microscopy are indicative of mutual interactions between semiconducting SWNTs and a water-soluble strong electron acceptor, i.e., perylenediimide. Significant is the stability and the strong electronic coupling of the perylenediimide/SWNT electron donor—acceptor hybrids. Several spectroscopic and spectroelectrochemical techniques, i.e., Raman, absorption, and fluorescence, confirmed that distinct ground- and excited-state interactions occur and that kinetically and spectroscopically well characterized radical ion pair states form within a few picoseconds.
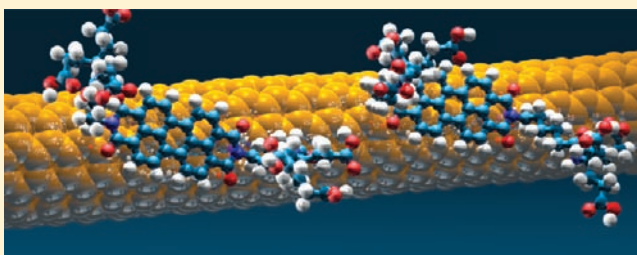
■ INTRODUCTION

The discovery of carbon nanostructures, such as fullerenes (C_{60}), single wall carbon nanotubes (SWNTs), and graphene, has triggered numerous investigations focusing on features that are relevant for applications in the fields of nanoelectronics, photovoltaics, etc.[1] In particular, for photovoltaic applications, the small reorganization energy that fullerenes exhibit in charge transfer reactions is of great value.[2] Ultrafast charge separation and slow charge recombination occur when fullerenes are involved, which results in exceptionally long-lived radical ion pair states.[3] In fact, the lifetime mirror-image has great potential for use in solar cells.[4]

The small diameters and the large aspect ratios of SWNTs render them ideal one-dimensional quantum wires, again a great asset for solar cells.[5] In contrast to fullerenes, however, real breakthroughs in the field of SWNTs are hindered by their poor solubility in aqueous and organic solvents.[6] SWNTs exist predominantly in aggregated forms, which usually alter their electronic and optical properties. Additionally, SWNTs are polydispersed in nature.[7] SWNTs are, for example, either metallic or semiconducting with different band gaps, but only the latter are of interest for the construction of nanoscale semiconductor devices.[8] To this end, the SWNT diameter inversely correlates with the absorption and emission energies and band gaps between their valence and conductance bands.[9] Despite these limitations, the combination of SWNTs and

electron acceptors generates photoactive materials, which can produce electrical energy when irradiated.[10]

An interesting aspect for charge transfer/photovoltaic applications is the control over the electronic properties of semiconducting SWNTs. However, what makes this task difficult is the detailed and unambiguous description of all the electronic features of individual SWNTs by means of near-infrared fluorescence, electrochemistry, etc. In this context, doping constitutes a powerful approach. It substantially increases the density of free charge carriers and, in turn, enhances the electrical and thermal conductivities.[11] Most notable is the reversible intercalation and deintercalation of electron-donating potassium/cesium or electron accepting iodine/bromine.[12] Here, the charge carriers change from holes to electrons and vice versa. Along the same lines, replacement of carbon by boron, nitrogen, or silicon has been shown to impact the electronic and transport properties of SWNTs.[13]

Light-induced doping with excited-state electron donors or electron acceptors is currently emerging as a versatile option in the field of SWNT doping. This process generates transient charge carriers in the conduction and valence bands of SWNTs, respectively. On one hand, the transfer of electrons from electron donors into the conduction bands of semiconducting SWNTs is
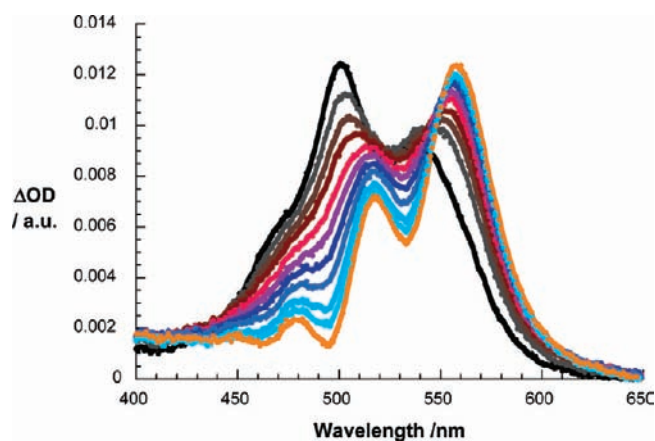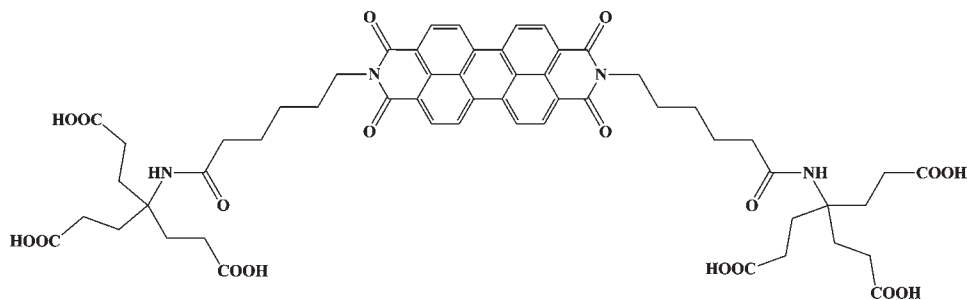
Chart 1

Figure 1. Absorption changes related to **1** in D_2O (7.5×10^{-5} M) in the presence of SWNTs versus time, starting at 5 min (black line) in 5 min steps up to 50 min (orange line) at room temperature.

Figure 2. Absorption changes related to SWNT in the presence of **1** in D_2O (7.5×10^{-5} M) after 50 min at room temperature.

well established.[14] On the other hand, the use of SWNTs as electron donors is still scarce. A key issue addresses the strategy to interface SWNTs with electron donors or electron acceptors. One strategy relies on the use of protocols to covalently attach electron donors or electron acceptors to SWNTs.[15] Here, the impact that the covalent functionalization exerts on the electronic structure is noticeable. Since the electron transport is ballistic for semiconducting SWNTs only over distances of a few hundred nanometers,[16] transport properties are affected by the covalent functionalization. An alternative strategy is based on noncovalent means to implement multifunctional groups. A noncovalent strategy preserves the electronic structure of SWNTs and is more straightforward than covalent strategies. Important contributions stem from $\pi-\pi$ interactions with amphiphilic polycyclic aromatic hydrocarbons.[17] They assist in realizing the control over the molecular composition of individual/separated SWNT electron-donor acceptor hybrids and provide water-solubility.[10,18]

In contrast to our previous work on HiPCO SWNTs,[10,14a,17c,17d] we focus in the current work on CoMoCAT SWNTs. The motivation to study this system originates from the following facts. CoMoCAT SWNTs feature high concentrations of (6,5) nanotubes, a narrow range of diameters, and a narrow range of chiral angles, and the concentration of semiconducting SWNTs is higher than 90%.[19] A detailed spectroscopic and microscopic study corroborates the charge transfer chemistry of pristine SWNTs, involving ground-state and excited-state interactions, using perylene dye **1**, which combines
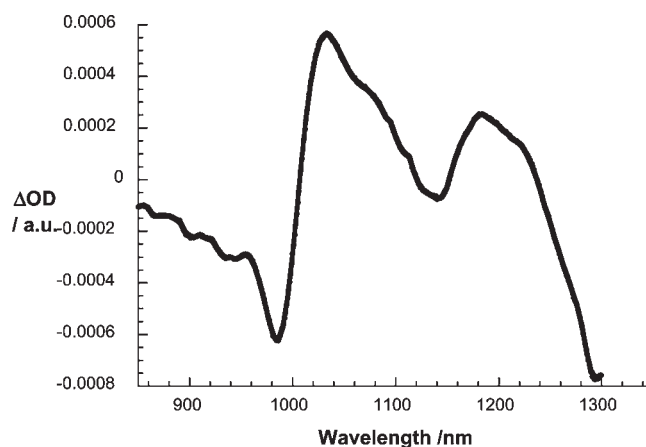
excellent electron-accepting features with a reasonably sized π-system.[10,18d−18f]

■ RESULTS AND DISCUSSION

Compound **1** (Chart 1) was prepared according to reported procedures.[20] In aqueous buffered media (pH 7.2, 10^{-2} M $H_2PO_4^-/HPO_4^{2-}$), **1** shows characteristics in the absorption spectrum that indicate the presence of aggregates (see Figure S1, Supporting Information). In particular, maxima and shoulders at 387, 475, 500, and 547 nm reflect the vibrational progression of **1**, however, with oscillator strength opposite to what is known for the monomer of **1**. The spectrum of SWNT/SDBS, on the other hand, is dominated by maxima at 980 (6,5), 1125 (7,6), and 1265 nm (8,7). Moreover, 570 (6,5) and 650 nm (7,6) maxima are discernible as well (see Figure S2, Supporting Information).[21]

When SWNT/SDBS are exposed to **1**, interactions between the SWNT and **1** are reflected in a slow transformation of the aggregates of **1** into that of the monomer which is independent of the presence of SDBS. Figure 1 documents, for example, that the 475, 500, and 543 nm features (attributed to the aggregated form) are replaced by 480, 515, and 558 nm maxima (i.e., monomer). Throughout this transformation the oscillator strength reverses, that is, the 558 nm maximum becomes stronger when compared to the 515 nm maximum. An overall bathochromic shift of 15 nm evolves relative to SWNT/**1**, due to $\pi-\pi$ interactions. When exceeding a SWNT to **1** ratio of 1:10 the resulting absorption spectra are best described as the simple superimposition of monomeric **1** and aggregated **1**; indicators
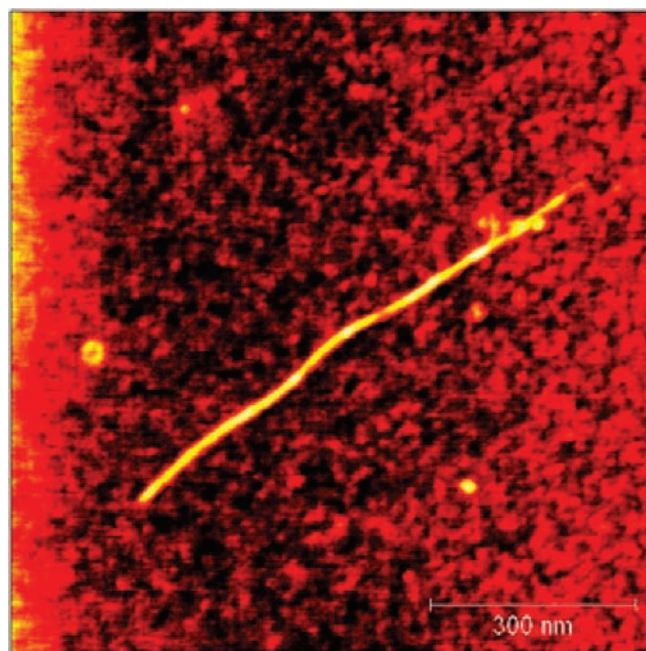
Figure 3. AFM image of SWNT/**1** on a silicon wafer deposited from a suspension in D_2O—buffer: pH 7.2, 10^{-2} M $H_2PO_4^-/HPO_4^{2-}$.
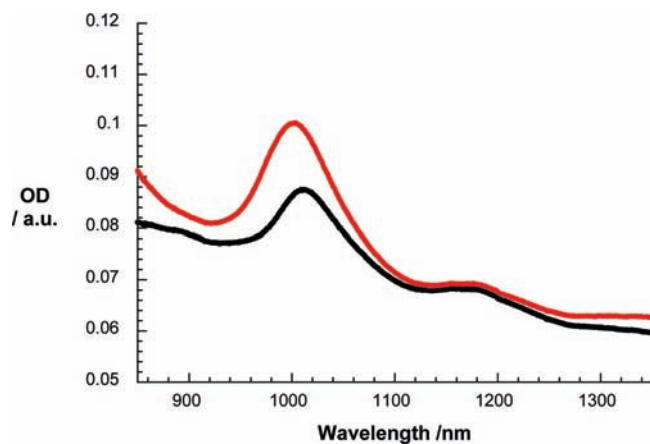

Figure 4. Absorption spectra of SWNT/**1** in D_2O—buffer: pH 7.2, 10^{-2} M $H_2PO_4^-/HPO_4^{2-}$, with applied potentials (vs Ag wire) of +0.2 V (black spectrum) and −0.6 V (red spectrum) under argon at room temperature.

Figure 5. in situ Raman/electrochemical spectra (λ_{ex} = 1064 nm, Nd: YAG Laser) with focus on the G′ region of SWNT/**1** D_2O—buffer: pH 7.2, 10^{-2} M $H_2PO_4^-/HPO_4^{2-}$, with applied potentials (vs Ag wire) of +0.2 V (black spectrum), −0.2 V (gray spectrum), and −0.6 V (red spectrum) under argon at room temperature.

To shed light onto the nature of the interactions, we turned to electrochemistry/spectroelectrochemistry. In particular, differential absorption changes were recorded upon oxidizing and reducing SWNT/SDBS as well as reducing and oxidizing SWNT/**1**. Upon oxidation (i.e., applying potentials of −0.6, −0.4, −0.2, 0.0, and +0.2 V vs Ag wire) of SWNT/SDBS in D_2O (5×10^{-3} M NaCl), the intensity of the M_{11} and S_{22} transitions in the 450 to 570 and 650 nm range, respectively, increases with applied potential, while that of the S_{11} absorptions in the 980 to 1170 range decreases relative to 0.0 V versus Ag wire (see Figure S5, Supporting Information). For SWNT/**1** in aqueous buffered media (pH 7.2, 10^{-2} M $H_2PO_4^-/HPO_4^{2-}$), on the other hand, under oxidative conditions, changes neither in the visible nor in the near-infrared of the absorption spectrum are discernible. Upon reduction of SWNT/SDBS, a contrasting behavior is noted. In particular, the region of the S_{11} transition, on one hand, is characterized by an overall increase of the absorptions, while the regions of the M_{11} and S_{22} transitions, on the other hand, are dominated by a general decrease of intensity. Figure 4 corroborates that during the electrochemical reduction of SWNT/**1**, that is, applying potentials of +0.2, 0, −0.2, −0.4, and −0.6 V, the S_{11} absorptions increase and shift hypsochromically. For example, the (6,5) maximum at 1010 nm is replaced by a 990 nm maximum. In other words, the chemically oxidized SWNTs, by charge transfer from **1**, are successfully reduced by charge transfer at the electrode. The overall trend is completely reversible as confirmed by the recovery of the original SWNT/**1** features upon changing the bias step-by-step from −0.6 to 0 V. Going, however, beyond this bias leads to an oxidation of **1** and a loss of doping.

Further support for SWNT doping, as a result of SWNT/**1**, came from Raman experiments. As gathered in Figure S4, Supporting Information, relative to SWNT/SDBS the RBM, G^+, and $G^\#$ modes in SWNT/**1** are shifted. In particular, the RBM resonances at 265 (6,5), 308 (7,5), and 329 (8,7) cm^{-1} shift to 269, 313, and 333 cm^{-1}, respectively, revealing the needs of higher activation energies. Similar blue-shifts are seen for the G^+ and $G^\#$ modes. Additionally, all of the Raman modes in SWNT/**1** tend to be much weaker relative to those of the SWNTs. In situ Raman/electrochemical experiments confirmed the reversibility of the SWNT doping. In SWNT/**1**, fairly weak

are hypsochromically shifted maxima and change in oscillator strength.

When turning to the near-infrared region as a complement to the visible range, we see that SWNTs are also susceptible to electronic interactions. During the course of the above experiments, the SWNT transitions shift incrementally to the red (see Figure S3, Supporting Information). In Figure 2, which displays differential absorption changes, bleaching of the 980, 1135, and 1285 transitions is accompanied by the formation of new maxima at 1030 and 1180 nm.[22]

Ensuring the homogeneity of SWNT/**1** is critical. In this context, atomic force microscopy is an important technique, since it provides important insights into this aspect. Figure 3 confirms that throughout the scanned areas predominantly short (i.e., 5 μm) and thin bundles (i.e., 1−2 nm) of SWNT/**1** are discernible.
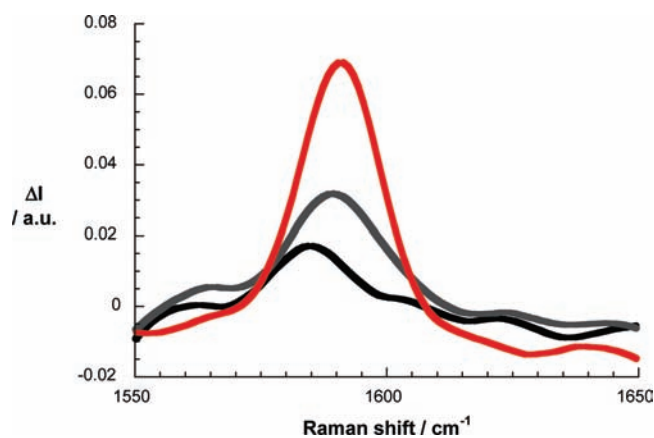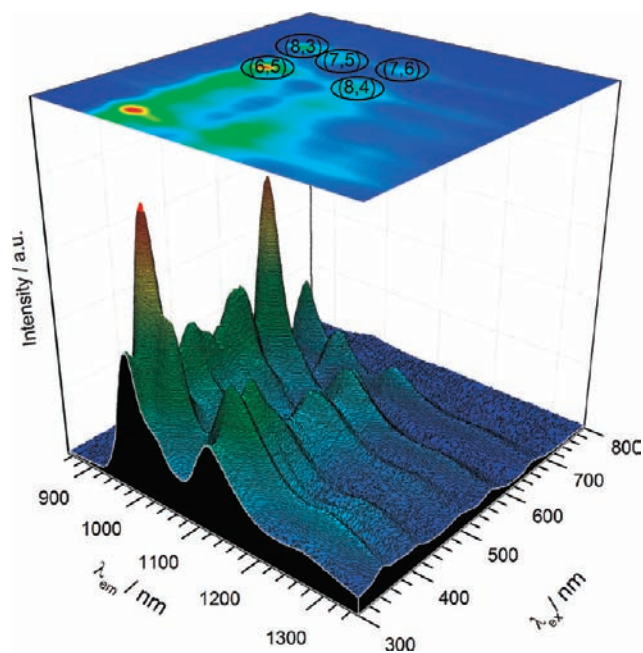
Figure 6. Steady-state fluorescence spectra, with increasing intensity from blue to green to yellow and to red, of SWNT/SDBS in D_2O dispersion at room temperature.
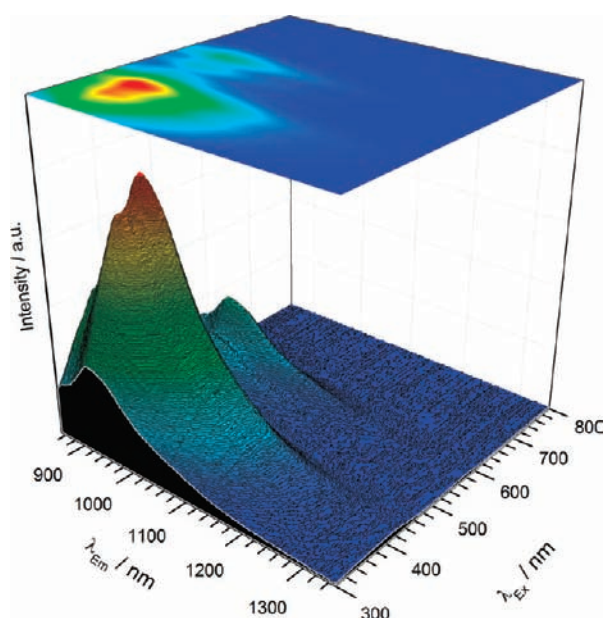

Figure 7. Steady-state fluorescence spectra, with increasing intensity from blue to green to yellow and to red, of SWNT/**1** in D_2O—buffer: pH 7.2, 10^{-2} M $H_2PO_4^-$/HPO_4^{2-}, at room temperature.

G^+ and $G^{\#}$ modes at 1585 and 2575 cm^{-1}, respectively, are replaced upon applying reductive bias (i.e., +0.4, 0, and −0.8 V) by much stronger resonances at 1591 and 2555 cm^{-1} (see Figure 5). In complementary experiments, namely oxidative bias for SWNTs, the trends are reversed: red-shifts and intensity decrease.

The conclusion of the aforementioned assays is a reversible doping of SWNTs in the ground state. To investigate the excited-state interactions, the fluorescence of **1** and SWNTs in the visible and near-infrared regions was probed in separate experiments. In
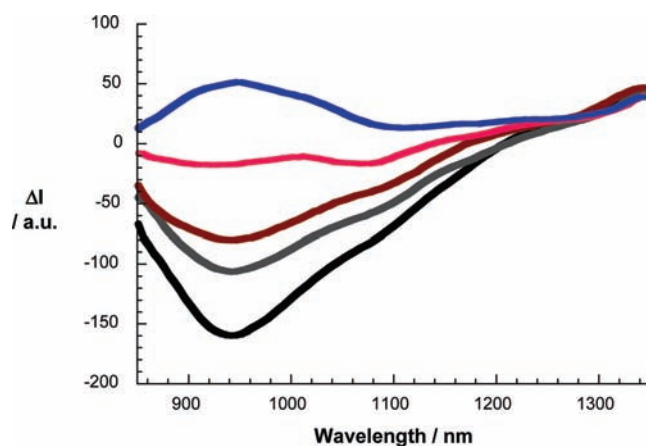

Figure 8. in situ fluorescence/electrochemical spectra (λ_{ex} = 676 nm, Kr Laser) of SWNT/**1** in D_2O—buffer: pH 7.2, 10^{-2} M $H_2PO_4^-$/HPO_4^{2-}, with applied potentials (vs Ag wire) from +0.2 V (black), 0.0 V (gray), −0.2 V (red), −0.4 V (pink) to −0.6 V (blue spectrum) under argon at room temperature.

the case of **1**, only the monomer exhibits the known fluorescence in the visible region with maxima at 550 and 590 nm and with quantum yields that depended on the buffer concentration up to 1. In the near-infrared region a broad emission band is observable with a shoulder at 860 nm and a maximum at 920 nm, which belongs to the aggregate, and overlays the emission of the SWNT. Nevertheless, in SWNT/**1** the emission of the surface-attached monomer is completely quenched, prompting to an efficient excited-state deactivation of **1** once immobilized onto the SWNT.[23]

The fluorescence of SWNT/SDBS is dominated by maxima at 955, 980, 1025, and 1120 nm, which correspond to (8,3), (6,5), (7,5), and (7,6), respectively.[21,24] A typical 3-D spectrum is reported in Figure 6. Under reductive conditions, that is, going gradually from +0.2 to −0.6 V (i.e., +0.2, 0, −0.2, −0.4, and −0.6 V), the previous SWNT-centered fluorescence decreases (Figure S6, Supporting Information). This trend is reversed when applying the opposite sequence, that is, −0.6, −0.4, −0.2, and 0 V. This reversibility is given throughout, at least, five different cycles.

In SWNT/**1**, the SWNT-centered features at 955, 980, 1025, and 1120 nm are substituted by broadened fluorescence maxima at 1045 (6,5) and 1190 nm (7,6) (see Figure 7 and Figure S7, Supporting Information. Besides the underlying red-shift, which mirror images the differences in the ground-state absorption spectra between the SWNT and SWNT/**1**, the fluorescence is quenched by a factor of approximately 100. At this stage, SWNT bundling/rebundling is ruled out due to the superior ability of **1** to suspend SWNTs, vide supra. As a matter of fact, we ascribe the fluorescence quenching to excited-state interactions, namely, electron transfer. On the other hand, a significant broadening and larger Stokes shifts, which are also seen, are likely to evolve from the charge transfer doping in SWNT/**1** and strongly interacting constituents.[25]

The aforementioned fluorescence of SWNT/**1** decreases upon going gradually from +0.2 to −0.6 V. Instead, a new fluorescence feature is maximized around 950 nm (see Figures 8). The maximum of the latter nearly coincides with that seen for SWNT/SDBS. Reverting the potentials step-by-step to −0.6, −0.4, −0.2, and finally to 0 V reestablished the original fluorescence spectrum of SWNT/**1**.
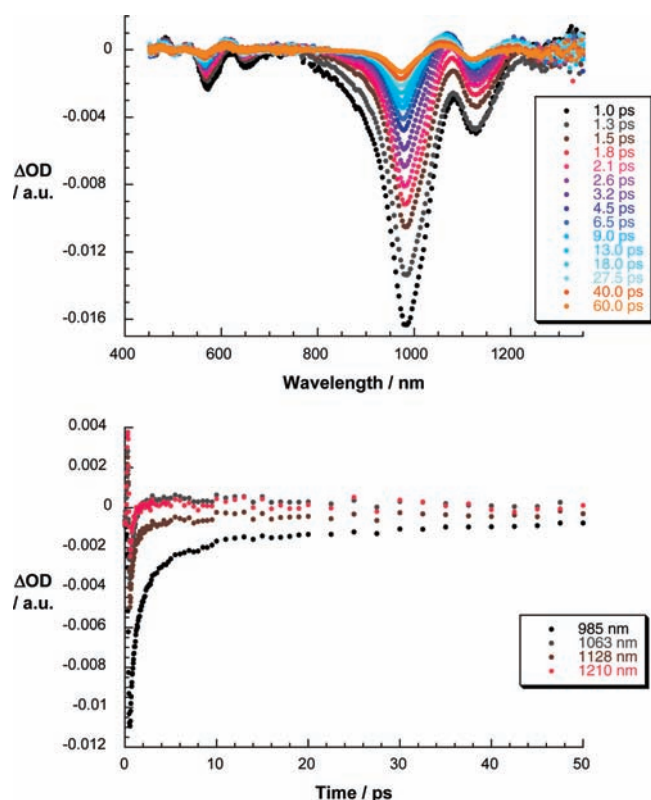
Figure 9. Upper part: differential absorption spectra (visible and near-infrared) obtained upon femtosecond flash photolysis (387 nm) of SWNT/SDBS in D_2O with several time delays between 0 and 60 ps at room temperature. Lower part: time-absorption profiles of the spectra at 985, 1063, 1128, and 1210 nm, monitoring the excited-state decay/ground-state recovery.

Figure 10. Upper part: differential absorption spectra (visible and near-infrared) obtained upon femtosecond flash photolysis (387 nm) of SWNT/**1** in D_2O—buffer: pH 7.2, 10^{-2} M $H_2PO_4^-$/HPO_4^{2-}, with several time delays between 0 and 60 ps at room temperature. Lower part: time-absorption profiles of the spectra at 1053 and 1138 nm, monitoring the charge separation and charge recombination.

Next, transient absorption measurements were performed with SWNT/SDBS and SWNT/**1** (compare Figures 9 and 10). For SWNT/SDBS, predominant features at 980, 1130, and 1270 nm, as they are recorded immediately upon 387 or 775 nm excitation (i.e., 0.5 ps), are a reasonable reflection of the ground-state absorptions, that is, (6,5), (7,5), and (8,7). In line with previous investigations, the decay of SWNT excited states is fast and multiexponential. Taking, for example, the 990 nm time absorption profile, a biexponential fitting affords major lifetimes of 2.5 and 45.6 ps. Throughout this temporal evolution, the 980, 1130, and 1270 nm characteristics blue-shift slightly (i.e., 980 to 976 nm) before the ground state is almost quantitatively recovered.

Following photoexcitation of SWNT/**1** at either 387 or 775 nm, we see in line with the absorption spectra the rapid formation of a transient bleach at 1045 and 1195 nm. Notable is also an appreciable broadening of the differential absorption changes when compared to SWNT/SDBS. Again, this trend mirror images the differences in the absorption spectra of SWNT/**1** and SWNT/SDBS. The aforementioned result attests to the selective excitation of SWNT/**1**. The latter transforms, however, with a lifetime of 4.5 ps into a new transient state. This newly formed transient reveals in the visible range a minimum and a maximum at 560 and 680 nm, respectively, which resemble the fingerprint of the one-electron radical anion of **1**. In the near-infrared, on the other hand, minima at 1015/1190 nm and a maximum of 1115 nm match the oxidized form of the SWNT.
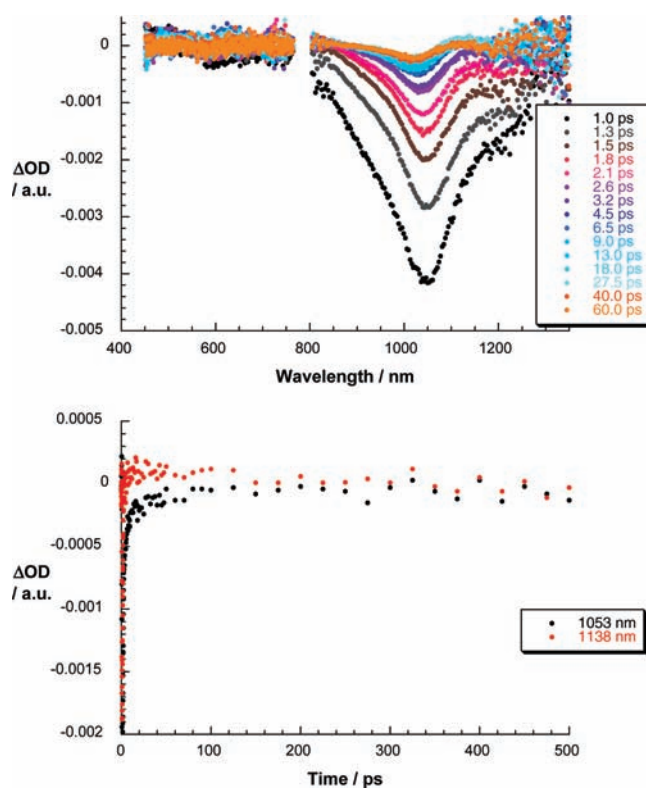
Taking the aforementioned result into concert, we conclude that the selective excitation of SWNT/**1**, in which sizable shifts of electron density prevail, is followed by a full separation of charges, namely reduction of **1** and oxidation of the SWNT. Owing to the strong interactions between SWNTs and **1**, the lifetime of reduced **1**/oxidized SWNT is limited to 170 ps.

■ CONCLUSIONS

In summary, by complementary spectroscopic and microscopic techniques, we could show mutual interactions between semiconducting SWNTs and a water-soluble, electron accepting perylene diimide. The establishment of a versatile methodology to achieve water-soluble SWNTs for processing under environmentally friendly conditions and further the embedding of such high stable perylenediimide/SWNT electron donor—acceptor hybrids is important for novel photovoltaic cells. Another relevant result of this study is that a wide range of complementary spectroscopies and also the use of new in situ spectroelectrochemistry techniques, Raman, absorption, and fluorescence spectroscopy, confirmed that distinct ground- and excited-state interactions occur and that kinetically and spectroscopically well characterized radical ion pair states are formed. Ground-state interactions are driven by $\pi-\pi$ stacking that are augmented by charge transfer interactions as evidenced by the in situ spectroelectrochemistry measurement. Overall, matching the n-type character of perylene diimide and the p-type character of SWNTs is a very important milestone for photovoltaic applications.

Currently, we are directing our attention to use this rather unique combination of perylene diimides and SWNTs for the fabrication of photovoltaic cells that are based on different nanocarbons.

EXPERIMENTAL SECTION

Syntheses. The synthesis of the water-soluble perylene **1** has been accomplished in the group of Professor Andreas Hirsch according to literature procedures.[20] The SWNTs (CoMoCat) were achieved by the group of Prof. Prato (Trieste/Italy) after less purification.

Spectroscopy, Spectroelectrochemistry, and Microscopy. Steady-state UV/vis/NIR absorption spectroscopy was performed on a Cary 5000 spectrometer (Varian). Transient absorption spectroscopy was performed with 775 and 387 nm laser pulses from an amplified Ti/sapphire laser system (Model CPA 2101, Clark-MXR Inc.; output: 775 nm, 1 kHz, and 150 fs pulse width) in the TAPPS (Transient Absorption Pump/Probe System) Helios from Ultrafast Systems with 200 nJ laser energy. Steady-state fluorescence spectra were taken from samples by a FluoroMax3 spectrometer (Horiba) in the visible detection range and by a FluoroLog3 spectrometer (Horiba) with a IGA Symphony (512 × 1 × 1 μm) detector in the NIR detection range. The Raman spectra were run with a FT-Raman spectrometer RFS100 from Bruker with an excitation wavelength of 1064 nm and a liquid nitrogen-cooled germanium detector. Spectroelectrochemistry experiments were performed with a home-built cell and a three-electrode setup: a light-transparent platinum gauze as working electrode, a platinum wire as counter electrode, and a silver wire as quasireference electrode. Potentials were applied and monitored with a HEKA Elektronik Potentiostat/Galvanostat PG284 and a Metrohm-Autolab Potentiostat/Galvanostat PGSTAT101. The path length of the cell was 2.3 mm. The results are finally shown as differential spectra, i.e., the difference between a spectrum with and without an applied potential. The spectra were recorded with a UV/vis/NIR-spectrometer Cary 5000 (Varian), a FT-Raman spectrometer RFS100 (Bruker), and a FluoroLog3 spectrometer (Horiba) with a IGA Symphony (512 × 1 × 1 μm) detector in the NIR detection range. AFM images were taken by samples which were prepared by spin-coating (3000 rpm, 6 min) onto silicon wafers from a SWNT dispersion and then investigated by using a Digital Instruments (Veeco) Nanoscope IIIa (Tapping Mode) with Veeco RTESP7 Tips.

ASSOCIATED CONTENT

ⓢ Supporting Information. Additional information as noted in the text. This material is available free of charge via the Internet at http://pubs.acs.org.

AUTHOR INFORMATION

Corresponding Author
andreas.hirsch@chemie.uni-erlangen.de; dirk.guldi@chemie.uni-erlangen.de

ACKNOWLEDGMENT

REFERENCES

(1) (a) *Carbon Nanotubes: Advanced Topics in the Synthesis, Structure, Properties and Applications*; Jorio, A.; Dresselhaus, G.; Dresselhaus, M. S., Eds.; Springer: Berlin, 2008. (b) *Carbon Nanotubes: Synthesis, Structure, Properties and Applications*; Dresselhaus, M. S.; Dresselhaus, G.; Avouris, P., Eds.; Springer: Berlin, 2001. (c) *The Science and Technology of Carbon Nanotubes*; Tanaka, K.; Yamabe, T.; Fukui, K., Eds.; Elsevier: Oxford, 1999. (d) *Carbon Nanotubes and Related Structures: New Materials for the Twenty-First Century*; Harris, P. J. F., Ed.; Cambridge University Press: Cambridge, 2001. (e) *Carbon Nanotubes and Related Structures*; Guldi, D. M.; Martin, N., Eds.; Wiley-VCH: Weinheim, 2010.

(2) (a) Imahori, H.; Tkachenko, N. V.; Vehmanen, V.; Tamaki, K.; Lemmetyinen, H.; Sakata, Y.; Fukuzumi, S. *J. Phys. Chem. A* **2001**, *105*, 1750. (b) Guldi, D. M. *J. Phys. Chem. B* **2005**, *105*, 11432.

(3) (a) Guldi, D. M.; González, S.; Martín, N.; Antón, A.; Garín, J.; Orduna, J. *J. Org. Chem.* **2000**, *65*, 1978. (b) Imahori, H.; Tamaki, K.; Guldi, D. M.; Luo, C.; Fujitsuka, M.; Ito, O.; Sakata, Y.; Fukuzumi, S. *J. Am. Chem. Soc.* **2001**, *123*, 2607.

(4) (a) Guldi, D. M.; Zilbermann, I.; Anderson, G.; Kotov, N. A.; Tagmatarchis, N.; Prato, M. *J. Mater. Chem.* **2005**, *15*, 114. (b) Sgobba, V.; Giancane, G.; Conoci, S.; Casilli, S.; Ricciardi, G.; Guldi, D. M.; Prato, M.; Valli, L. *J. Am. Chem. Soc.* **2007**, *129*, 3148.

(5) (a) Sgobba, V.; Rahman, G. M. A.; Guldi, D. M.; Jux, N.; Campidelli, S.; Prato, M. *Adv. Mater.* **2006**, *18*, 2264. (b) Campidelli, S.; Klumpp, C.; Bianco, A.; Guldi, D. M.; Prato, M. *J. Phys. Org. Chem.* **2006**, *19*, 531. (c) Sgobba, V; Guldi, D. M. *Chem. Soc. Rev.* **2009**, *38*, 165.

(6) (a) Bahr, J. L.; Mickelson, E. T.; Bronikowski, M. J.; Smalley, R. E.; Tour, J. M. *Chem. Commun.* **2001**, 193. (b) Ausman, K. D.; Piner, R.; Lourie, O.; Ruoff, R. S.; Korobov, M. *J. Phys. Chem. B* **2000**, *104*, 8911.

(7) (a) Fujigaya, T.; Nakashima, N. *Polym. J.* **2008**, *40*, 577. (b) Bergin, S. D.; Sun, S.; Rickard, D.; Streich, P. V.; Hamilton, J. P.; Coleman, J. N. *ACS Nano* **2009**, *3*, 2340. (c) Moonoosawmy, K. R.; Kruse, P. *J. Am. Chem. Soc.* **2008**, *130*, 13417.

(8) Campidelli, S.; Meneghetti, M; Prato, M. *Small* **2007**, *3*, 1672.

(9) (a) *Carbon Nanotubes*; Endo, M.; Iijima, S.; Dresselhaus, M. S., Eds.; Elsevier: Oxford, 1996. (b) *Carbon Nanotubes in Topics - Applied Physics 111*; Jorio, A.; Dresselhaus, M. S.; Dresselhaus, G., Eds.; Springer: Berlin, 2008.

(10) Ehli, C.; Oelsner, C.; Guldi, D. M.; Mateo-Alonso, A.; Prato, M.; Schmidt, C.; Backes, C.; Hauke, F.; Hirsch, A. *Nat. Chem.* **2009**, *1*, 243.

(11) Carrol, D. L.; Redlich, Ph.; Blase, X.; Charlier, J.-C.; Curran, S.; Ajayan, P. M.; Roth, S.; Rühle, M. *Phys. Rev. Lett.* **1998**, *81*, 2332.

(12) (a) Fischer, J. E. *Acc. Chem. Res.* **2002**, *35*, 1079. (b) Chun, K.-Y.; Lee, C. J. *J. Phys. Chem. C* **2008**, *112*, 4492. (c) Michel, T.; Alvarez, L.; Sauvajol, J.-L.; Almairac, R.; Aznar, R.; Mathon, O.; Bantignies, J.-L.; Flahaut, E. *J. Phys. Chem. Solids* **2006**, *67*, 1190. (d) Rao, C. N. R.; Voggu, R. *Mater. Today* **2010**, *13*, 34.

(13) (a) Blackburn, J. L.; Yan, Y.; Engtrakul, C.; Parilla, P. A.; Jones, K.; Gennett, T.; Dillon, A. C.; Heben, M. *J. Chem. Mater.* **2006**, *18*, 2558. (b) Maciel, I. O.; Campos-Delgado, J.; Pimenta, M. A.; Terrones, M.; Terrones, H.; Rao, A. M.; Jorio, A. *Phys. Status Solidi B* **2009**, *246*, 2432.

(14) (a) Herranz, M. A.; Martín, N.; Campidelli, S.; Prato, M.; Brehm, G.; Guldi, D. M. *Angew. Chem., Int. Ed.* **2006**, *45*, 4478. (b) Li, H.; Zhou, Z.; Lin, Y.; Gu, L.; Wang, W.; Shiral Fernando, K. A.; Kumar, S.; Allard, L. F.; Sun, Y.-P. *J. Am. Chem. Soc.* **2004**, *126*, 1014. (c) Guldi, D. M.; Marcaccio, M.; Paolucci, D.; Paolucci, F.; Tagmatarchis, N.; Tasis, D.; Vazquez, E.; Prato, M. *Angew. Chem., Int. Ed.* **2003**, *42*, 4206.

(15) (a) Tasis, D.; Tagmatarchis, N; Bianco, A.; Prato, M. *Chem. Rev.* **2006**, *106*, 1105. (b) Li, H.; Martin, B. A.; Harruff, B. A.; Carino, R. A.; Allard, L. F.; Sun, Y.-P. *Adv. Mater.* **2004**, *16*, 896. (c) Baskaran, D.; Ways, J. W.; Zhang, X. P.; Bratcher, M. S. *J. Am. Chem. Soc.* **2005**, *127*, 6916. (d) Singh, P.; Campidelli, S.; Giordani, S.; Bonifazi, D.; Bianco, A.; Prato, M. *Chem. Soc. Rev.* **2009**, *38*, 2214. (e) Brunetti, F. G.; Herrero, M. A.; Munoz, J. d. M.; Diaz-Ortiz, A.; Alfonsi, J.; Meneghetti, M.; Prato, M.; Vazquez, E. *J. Am. Chem. Soc.* **2008**, *130*, 8094.

(16) (a) White, C. T.; Todorov, T. N. *Nature* **1998**, *393*, 240. (b) Dekker, C. *Phys. Today* **1999**, 22. (c) McEuen, P. L.; Park, J.-Y. *Mater. Res. Soc.* **2004**, *29*, 272. (d) Bockrath, M.; Cobden, D. H.; McEuen, P. L.; Chopra, N. G.; Zettl, A.; Thess, A.; Smalley, R. E. *Science* **1997**, *275*, 1922.

4585

dx.doi.org/10.1021/ja1108744 |*J. Am. Chem. Soc.* 2011, 133, 4580–4586

(17) (a) Murakami, H.; Nomura, T.; Nakashima, N. N. *Chem. Phys. Lett.* **2003**, *378*, 481. (b) Britz, D. A.; Khlobystov, A. N. *Chem. Soc. Rev.* **2006**, *35*, 637. (c) Mateo-Alonso, A.; Ehli, C.; Chen, K. H.; Guldi, D. M.; Prato, M. *J. Phys. Chem. A* **2007**, *111*, 12669. (d) Ehli, C.; Guldi, D. M.; Herranz, M. A.; Martin, N.; Campidelli, S.; Prato, M. *J. Mater. Chem.* **2008**, *18*, 1498. (e) Herranz, M. A.; Ehli, C.; Campidelli, S.; Gutiérrez, M.; Hug, G. L.; Ohkubo, K.; Fukuzumi, S.; Prato, M.; Martin, N.; Guldi, D. M. *J. Am. Chem. Soc.* **2008**, *130*, 66.

(18) (a) Tomonari, Y.; Murakami, H.; Nakashima, N. *Chem.—Eur. J.* **2006**, *12*, 4027. (b) Chen, J.; Collier, C. P. *J. Phys. Chem. B* **2005**, *109*, 7605. (c) Nakashima, N.; Tomonari, Y.; Murakami, H. *Chem. Lett.* **2002**, *31*, 638. (d) Backes, C.; Schmidt, C. D.; Hauke, F.; Bottcher, C.; Hirsch, A. *J. Am. Chem. Soc.* **2009**, *131*, 2172. (e) Backes, C; Mundloch, U.; Ebel, A.; Hauke, F.; Hirsch, A. *Chem.—Eur. J.* **2010**, *16*, 3314. (f) Backes, C; Schmidt, C. D.; Rosenlehner, K; Hauke, F.; Coleman, J. N.; Hirsch, A. *Adv. Mater.* **2010**, *22*, 788. (g) Guldi, D. M.; Rahman, G. M. A.; Zerbetto, F.; Prato, M. *Acc. Chem. Res.* **2005**, *38*, 871.

(19) (a) Resasco, D.; Alvarez, W.; Pompeo, F.; Balzano, L.; Herrera, J.; Kitiyanan, B.; Borgna, A. *J. Nanopart. Res.* **2002**, *4*, 131. (b) Weisman, R. *Ind. Phys.* **2004**, *10*, 24.

(20) Schmidt, C. D.; Böttcher, C.; Hirsch, A. *Eur. J. Org. Chem.* **2007**, 5497.

(21) Bachilo, S. M.; Michael, S.; Strano, M. S.; Kittrell, C.; Hauge, R. H.; Smalley, R. E.; Weisman, R. B. *Science* **2002**, *298*, 2361.

(22) Addition of SDBS to SWNT/**1** leads to a replacement of **1** from the SWNT surface, and the features of pristine SWNTs are quantitatively recovered.

(23) The aggregate emission is neglected in this context.

(24) Hartschuh, A.; Pedrosa, H.; Peterson, J.; Huang, L.; Anger, P.; Qian, H.; Meixner, A.; Steiner, M.; Novotny, L.; Krauss, T. *ChemPhysChem* **2005**, *6*, 577.

(25) (a) Guldi, D. M.; Sgobba, V. *Chem. Commun* **2011**, 606. (b) Bartelmess, J.; Ehli, C.; Cid, J.-J.; Garcia Iglesias, M.; Vazquez, P.; Torres, T.; Guldi, D. M. *Chem. Sci.* **2011**, DOI: 10.1039/C0SC00364F.